Journal of Fluids and Structures 46 (2014) 77–88

Contents lists available at ScienceDirect

Journal of Fluids and Structures

journal homepage: www.elsevier.com/locate/jfs

Three-dimensional effects on the translational locomotion of a passive heaving wing

Jianxin Hu, Qing Xiao *

Department of Naval Architecture and Marine Engineering, University of Strathclyde, 100 Montrose Street, G4 0LZ Glasgow, United Kingdom

ARTICLE INFO

Article history:
Received 8 June 2013
Accepted 29 December 2013
Available online 7 February 2014

Keywords:
CFD
Passive flapping wing
Three-dimensional effect

ABSTRACT

This study was carried out on a three-dimensional wing with a freedom in translational direction under a prescribed up and down heaving motion. The investigation focused on how the system kinematics and structural parameters affect the dynamic response of a wing with a relatively small span length. The induced wing motion is a result of the system stability breakdown, which has only been observed by previous researches in the two-dimensional case. The results obtained indicate that the evolution of the wing locomotion is controlled not only by the flapping frequency but also influenced by the system inertia as well as the wing aspect ratio and density ratio. Moreover, initial perturbation effect on wings flexibility plays a role in the evolution development.

1. Introduction

The term “flapping” is always mentioned and employed in the study of wing motion of various animal species. In the classic studies, it is simplified to a combined pitching and heaving motion, and propulsion performance can be observed by examining the lateral fluid forces under a prescribed heaving or pitching motion numerically and experimentally (Triantafyllou et al., 1992; Lewin and Hajhariri, 2003; Dong et al., 2006; Heathcote and Gursul, 2007; Young and Lai, 2007; Tian et al., 2013).

In recent decades, attention has been focused on the propulsion mechanism under a coupled interaction between animal locomotion and its surrounding viscous fluid. In this context, the propulsion motion of animal is purely determined by the fluid force and moment generated by its forced locomotion. This is usually called, passive and self-propelled locomotion (Vandenberghe et al., 2004, 2006; Alben and Shelley, 2005; Lu and Liao, 2006; Spagnolie et al., 2010; Hu et al., 2011). Investigations are carried out by the foils with simple geometries, covering various system kinematic and structural parameters, such as foil shape, plunging frequency (f), amplitude (hc) and density ratio (σ). Results from these studies showed that the forced plunging motion leads to a symmetric foil moving in the direction perpendicular to the prescribed motion.

Although some research has been done in this self-propelled foil area, most of the above studies are focused on a large aspect ratio flapping wing. Therefore, a two-dimensional (2-D) assumption is reasonably valid, which significantly reduces the computational challenge and time. However, real aquatic animal fins may have relatively small aspect ratios such as the aspect ratios of four species of labrid fishes ranging from about 1.5 to 3.5 (Walker and Westneat, 2002), whereas bluegill sunfish and ratfish having pectoral fins with aspect ratios of about 2.4 (Drucker and Lauder, 1999) and 2.2 (Combes and Daneil, 2001), respectively, where three-dimensional (3-D) effect must be taken into account. Limited research on a 3-D

* Corresponding author.
E-mail address: qing.xiao@strath.ac.uk (Q. Xiao).

0889-9746/$ - see front matter © 2014 Elsevier Ltd. All rights reserved.
http://dx.doi.org/10.1016/j.jfluidstructs.2013.12.012

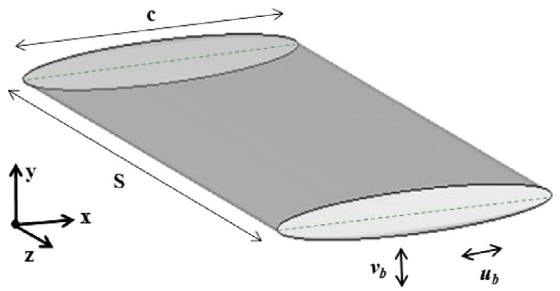

Fig. 1. Sketch of wing with an elliptical cross-section. The span is S and chord length c. The ratio of thickness to chord length is 0.1. It has a prescribed transverse velocity v_b and an induced translational velocity u_b.

tethered flapping wings shows that the wing with low aspect ratio generates high propulsion efficiency and reduced bending moment relative to the large aspect ratio wings (Walker and Westneat, 2002; Dong et al., 2006; Visbal et al., 2013).

The aim of present study is therefore to extend our recent work for a 2-D flapping foil with one degree of freedom (1-DoF) in translational direction, to a 3-D wing under low aspect ratio condition. Fig. 1 shows the wing under current investigation, a 3-D rectangular wing with an elliptical cross-section. The ratio of thickness to chord length is 0.1, and the aspect ratio is defined as AR$=S/c$, where S is the wing span (wing tip to tip distance) and c is the chord length. Instead of a tethered flapping motion, the wing is allowed to move in lateral direction. It has a freedom in in-line (x) direction, which is solely determined by the fluid-motion coupling between fluid and wing.

Investigation is first carried out on comparing the evolution process of left-right symmetric wing with large and medium aspect ratios, which are treated by 2-D and 3-D respectively. As the wing propulsion performance can be determined by variation of flapping wing′s kinematics and structural dynamic parameters, the examination on how such phenomena are influenced by structural and kinematic parameters are important. Therefore, we further discuss this self-propelled phenomenon in the aspects of 3-D effect, density ratio effect and perturbation effect on the induced in-line(x) direction locomotion ability. Wake structures of wings are presented with different aspect ratios, and the dynamic behaviors and propulsive properties of passive plunging wing is further analyzed in terms of typical kinematic quantities, such as the mean horizontal speed and the Strouhal number (St). To simplify the problem, at this stage, only the in-line freedom of wing is considered, while the freedom in pitch direction is not allowed. Detailed investigations on a 3-D wing with combined pitch and in-line freedom are published on another relevant paper (Xiao et al., 2014).

2. Mathematic models and validations

2.1. Fluid-motion coupling model

Referred to Fig. 1, the wing motions $\mathbf{u}_b=(u_b, v_b, 0)$ are explained as follows:

1. A specified sinusoidal plunging motion v_b:
$$v_b(t)=hc\omega \sin(\omega t), \tag{1}$$
where h is the non-dimensional flapping amplitude, ω is the flapping angular frequency, and $\omega=2\pi f$, where f is the flapping frequency;
2. An induced velocity u_b which is solely determined by the unsteady fluid forces through Newton′s second law:
$$m_b\frac{du_b}{dt}=F_x, \tag{2}$$
where m_b is the mass of wing, F_x is the hydrodynamic force in X direction including both pressure force and viscosity force. The density ratio σ is defined as the ratio between the density of wing and fluid, and $m_b=\sigma\rho V$, where V is the volume of the wing.

The instantaneous propulsion velocity u_b is obtained by integrating Eq. (2) with a first-order explicit scheme
$$u_b^t=\frac{F_x^{t-\Delta t}}{m_b}\Delta t+u_b^{t-\Delta t}, \tag{3}$$
where u_b^t and $u_b^{t-\Delta t}$ are X direction velocities at time instants t and $t-\Delta t$.

The fluid motion is governed by 3-D incompressible continuity and momentum equations as
$$\nabla\cdot\mathbf{u}=0,$$
$$\frac{\partial\mathbf{u}}{\partial t}+\mathbf{u}\cdot\nabla\mathbf{u}=-\frac{1}{\rho}\nabla p+\frac{\mu}{\rho}\nabla^2\mathbf{u}, \tag{4}$$
where $\mathbf{u}=(u, v, w)$ is the fluid velocity, p is the fluid pressure, μ is the fluid viscosity and ρ is the fluid density.

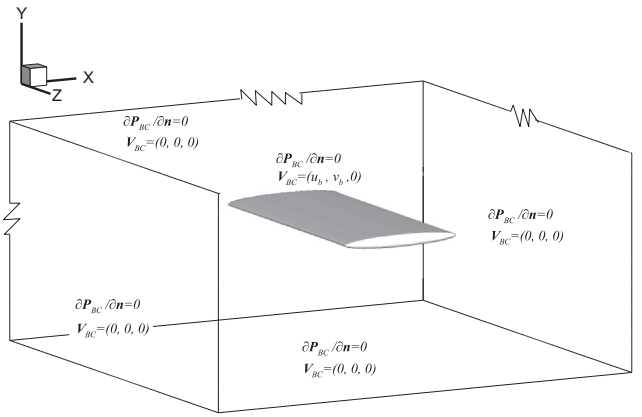

Fig. 2. Computational domain and boundary conditions. The domain size is 21, 11 and 18 of wing chord length (c) in X, Y and Z directions respectively. The fluid velocity and pressure are set as zero over all boundaries, and the wing surface is set as no slip wall, with kinematic motions (u_b, v_b).

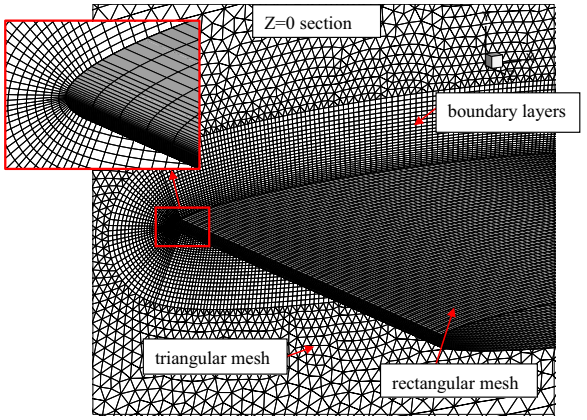

Fig. 3. Grid distribution over wing surface. In $Z=0$ section, the wing is covered by fine boundary layer mesh in the near surface area, and surrounded with triangular mesh in the outside area. The rectangular mesh distributes over the wing surface. By stretching cells in $Z=0$ section along Z direction, hexahedral and wedge mesh elements are generated over the domain space.

The flow field is simulated using the commercial CFD package FLUENT version 12.1.4. The computational domain is 21, 11 and 18 of wing chord length in in-line (x), transverse (y) and span-wise (z) directions, as shown in Fig. 2. Computational boundary conditions are set with fluid velocity and pressure disturbance to be zero, and no-slip wall boundary condition is used on the wing surface. Initial fluid velocity is set to be zero everywhere in the domain. The body's plunging motion (v_b) is imposed on the domain using Dynamic Mesh Function in FLUENT. To avoid mesh deformation and cope with the wing motion, the entire computational domain moves with wing as a rigid body.

The mesh over the wing is shown in Fig. 3. Structured mesh is used near the wing surface. Both rectangular and triangular grids are distributed over the section of $z=0$, and hexahedral and wedge mesh elements are generated along z direction. A non-symmetric mesh is distributed over the wing surface along z direction and x direction. In particular, near wing tip area, the mesh is specially refined to ensure the grid numbers are sufficient to precisely capture the unsteady wing tip vortex.

The schematic diagram for fluid and wing body motion coupling is shown in Fig. 4. At each time step, the simulation starts by updating body position by velocity v_b with the dynamic mesh function, which is also applied in our previous study (Xiao et al., 2011). Then the fluid evolution is solved by an unsteady incompressible solver with second-order upwind spatial discretization on Eq. (4). The flow field is assumed to be laminar as the induced translational Reynolds number (Re_u) is relatively small. The first-order implicit discretization is used for unsteady time marching, which is limited by the dynamic mesh adopted in FLUENT. The surface forces over wing is computed by Eq. (4), which can be used as an input by Eq. (3), by this way, an updated velocity u_b is obtained for the next time step.

The non-dimensional X direction force coefficient C_{Fx} is defined as

$$C_{Fx} = \frac{F_x}{\frac{1}{2}\rho(f(hc))^2 cL}, \tag{5}$$

where F_x is the hydrodynamic force in translational direction, L is the characteristic length assuming one unit herein.

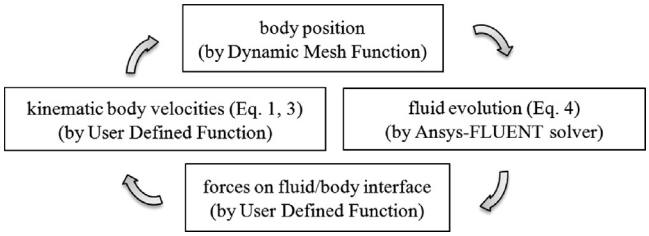

Fig. 4. Schematic diagram for fluid and wing body motion coupling.

Cycle-averaged input power P_{input} and input power coefficient C_p are calculated by the following equation:

$$P_{\text{input}} = f\int_{t}^{t+T} v_b(t)F_y\,dt, \quad C_P = \frac{P_{\text{input}}}{\frac{1}{2}\rho(f(hc))^2c^2L} \tag{6}$$

where F_y is the hydro-force in transverse direction.

Two Reynolds numbers are defined here, depending on the various velocities:

(a) Frequency Reynolds number Re_{fr}:

$$\text{Re}_{fr} = \frac{\rho f(hc)c}{\mu}. \tag{7}$$

(b) Instant translational Reynolds number Re_u:

$$\text{Re}_u = \frac{\rho c|\overline{u}_b|}{\mu}, \tag{8}$$

where $|\overline{u}_b|$ is the absolute value of mean horizontal speed u_b in the quasi-steady status.

Instantaneous non-dimensional translational velocity U is

$$U = \frac{u_b}{f(hc)}. \tag{9}$$

Strouhal number St is defined as

$$\text{St} = \frac{2\text{Re}_{fr}}{\text{Re}_u}. \tag{10}$$

2.2. Grid independence and validation

A grid and time step size independence test is conducted with a fine grid and a medium grid, and two time step sizes, $T/200$ and $T/400$ (T is the prescribed flapping cycling period), as the following three cases:

Case 1 (AR1.5-F): 180 intervals over the elliptical edge and 120 intervals along the span-wise edge, totally 4 535 550 mesh elements, time step size $T/200$.

Case 2 (AR1.5-M): 130 intervals over the elliptical edge and 80 intervals along the span-wise edge, totally 1 281 140 mesh elements; time step size $T/200$.

Case 3 (AR1.5-MT): 130 intervals over the elliptical edge and 80 intervals along the span-wise edge, totally 1 281 140 mesh elements; time step size $T/400$.

Computational results of the instantaneous drag force C_{Fx} are shown in Fig. 5, indicating a close result between the medium mesh and the fine mesh and these two time steps. Therefore the medium grid and the $T/200$ time step are used for all computations to ensure accuracy and minimize the time and memory consumption.

Due to an explicit time-marching scheme adopted in in-line x direction (Eq. (3)), the maximum time step is restricted under scheme stability constrains. It is also a function of grid numbers. For example, with a medium mesh number of 1 281 140, the maximum time step is $T/200$. To ensure the problem converges to an acceptable level, we monitored the iterating convergent history at each physical time step. The iteration steps are set until the momentum equation residual reducing three magnitudes.

To validate our developed numerical strategies, two test cases are performed. The first one is for a forced 3-D plunging wing studied previously by Guerrero (2009). The results are shown in Fig. 6(a) indicating a consistency with Guerrero (2009). The second validation test is carried out on a 2-D self-propelled (1-DoF) foil with a prescribed heave motion while freely movement in in-line x direction (Alben and Shelley, 2005). This problem is adopted for verifying the capability for our in-house developed UDF to deal with a coupled fluid–structure-interaction problem. In Fig. 6(b), the in-line induced velocity

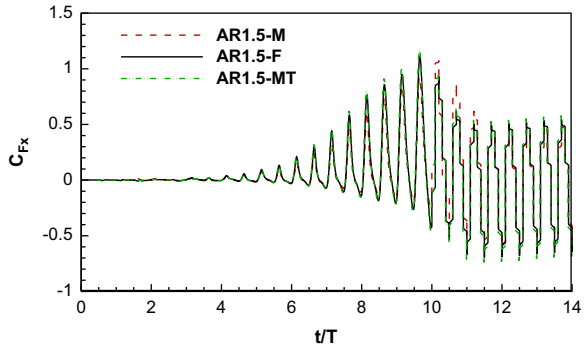

Fig. 5. Mesh and time step sensitivity study for three-dimensional wing ($h=0.5$, AR$=1.5$, Re$_{fr}=60$, $\sigma=4.0$). AR1.5-M: medium mesh with $dt=T/200$; AR1.5-F: fine mesh with $dt=T/200$; AR1.5-MT: medium mesh with $dt=T/400$.

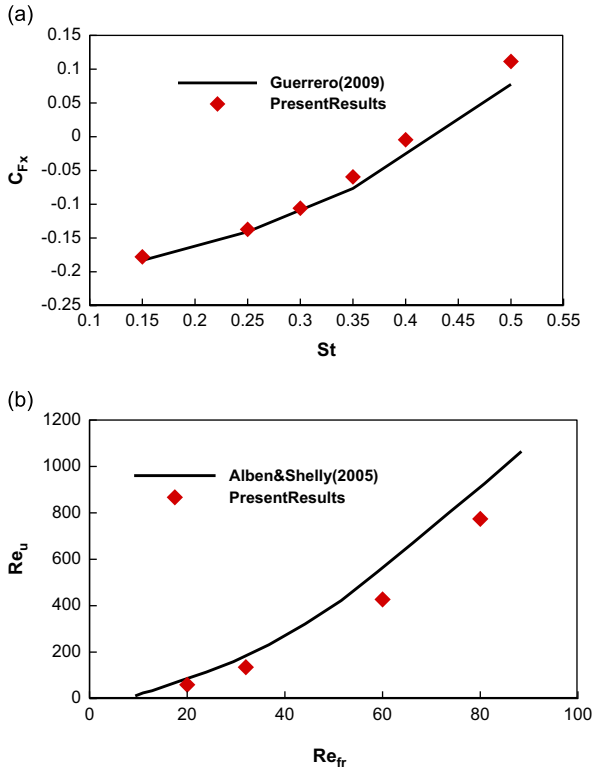

Fig. 6. Comparison with previous work. (a) Guerrero (2009) (AR$=1.0$, Re$=500$); (b) Alben and Shelley (2005) ($\sigma=32$, AR$=\infty$, $h=0.5$).

(Re$_u$) is compared with Alben and Shelley's data. The range of Re$_{fr}$ varies from 20 to 80, and the present results show a good agreement at low Re$_{fr}$, but with the under-estimated Re$_u$ at large flapping frequency. This is probably due to the different numerical methods used in two studies. Unfortunately, no other relevant simulation or experimental data are available for our comparison.

3. Results and discussion

In this section, the results of a parametric study are presented on the dynamical behavior of a wing with 1-DoF in lateral direction as mentioned above, and the comprehensive discussion is carried out. Amplitude h, aspect ratio AR, frequency Reynolds number Re$_{fr}$ and mass ratio σ are investigated and summarized in Table 1. The non-dimensional flapping amplitude h is simplified at 0.5, Re$_{fr}$ ranges in 20–80 and σ is between 4 and 32, which are consistent with other previous work (Lu and Liao, 2006; Miller and Peskin, 2004; Spagnolie et al., 2010; Zhang et al., 2010), where these parameters were

Table 1
Parameters list of self-propelled flapping wing.

Parameters	Values
h	0.5
Re_{fr}	20, 32, 45, 60, 80
AR	∞, 0.5, 1.0. 1.5, 2.0, 4.0, 6.0
σ	4, 6, 7, 8,10, 20, 32

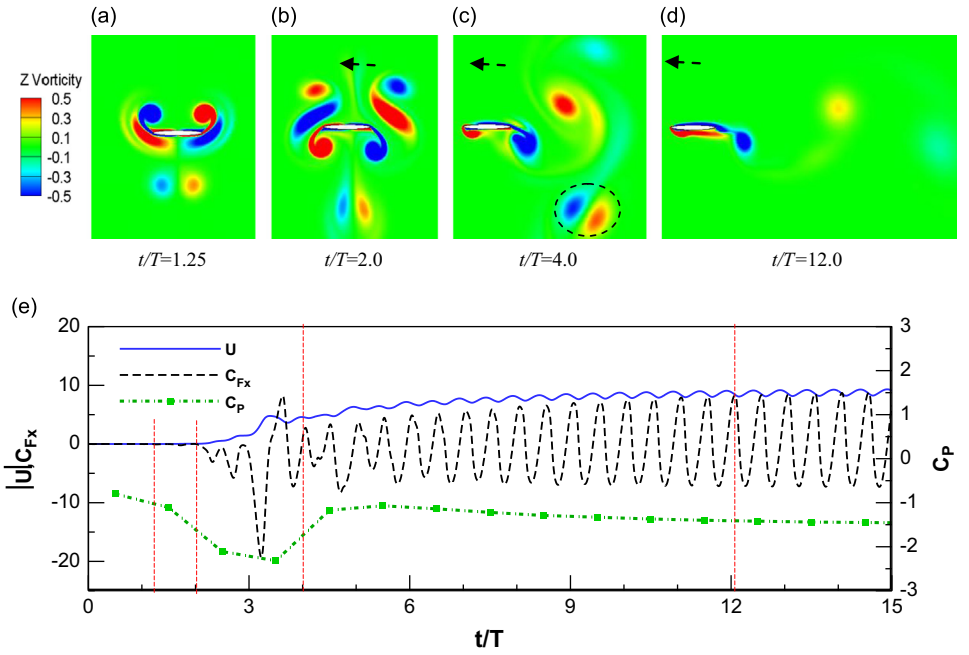

Fig. 7. Evolution process for a symmetric foil with AR$=\infty$ (2-D), $Re_{fr}=80$, $\sigma=4.0$. (a)–(d) Vortex topology at four instants (dashed arrows present traveling direction, and dashed circle presents vortex dipole); (e) instantaneous horizontal velocity, fluid force and the cycle-averaged-input power coefficient.

motivated by the real animal locomotion. Aspect ratios (0.5–∞) are varied to explore a 3-D effect, and the infinite large aspect ratio wing represents a 2-D wing.

3.1. Evolution process

In the past, the propulsion mechanisms of how locomotion transduces from the oscillation into translational motion in stationary water have been well studied by the 2-D symmetric foil, and an interesting phenomenon of symmetry breaking is well documented in the previous studies (Vandenberghe et al., 2004, 2006; Alben and Shelley, 2005; Lu and Liao, 2006). To describe the evolution process of a 3-D wing (AR$=4.0$) in comparison with a 2-D foil (AR$=\infty$), vorticity contours at four instants, fluid forces, lateral velocities and cycle-averaged-input powers are plotted in Figs. 7 and 8, where the result of a 3-D wing is quantified same as that of a 2-D foil under same Re_{fr} and σ. Since the direction of induced lateral motion is randomly selected, the moduli of velocity are used for presenting the evolution process and ensuring that a positive Re_u is always obtained. In the case of negative in-line x movement, a reflection plot of the vortex topology is presented.

It can be seen that the evolution mechanisms of a wing (AR$=4.0$, in 3-D) is pretty similar as a foil (AR$=\infty$, in 2-D). In particular, at early stage, both the foil and the wing plunge with a flow structure being left–right symmetric as typically shown in Figs. 7 and 8(a). At this stage, the net force in the in-line direction is nearly zero. As there is no constraint in translational direction, any small flow disturbance near the wing will cause the asymmetric flow structure and eventually leads to the foil/wing moving to one side (Figs. 7 and 8(b)). Once the wing starts to move, a transit period is needed before it finally reaches to a stable state, within which the vortex collides with others, resulting in a vortex dipole (as the dashed circle in Figs. 7 and 8(c)) which carries asymmetric suction forces at left and right edges. Consequently, horizontal forces vibrate with amplified amplitudes, leading to increased accelerations, and further causing rapidly increasing horizontal velocities. Finally, a stable translational locomotion is achieved as the wake being a reversed von Karman structure (Fig. 7(d)) or elongated ring loops (Fig. 8(d)), and both the velocity and the force vary periodically, with net forces being zero. The developing time and translational directions are sensitive to the initial conditions as we will show later. Meanwhile, the

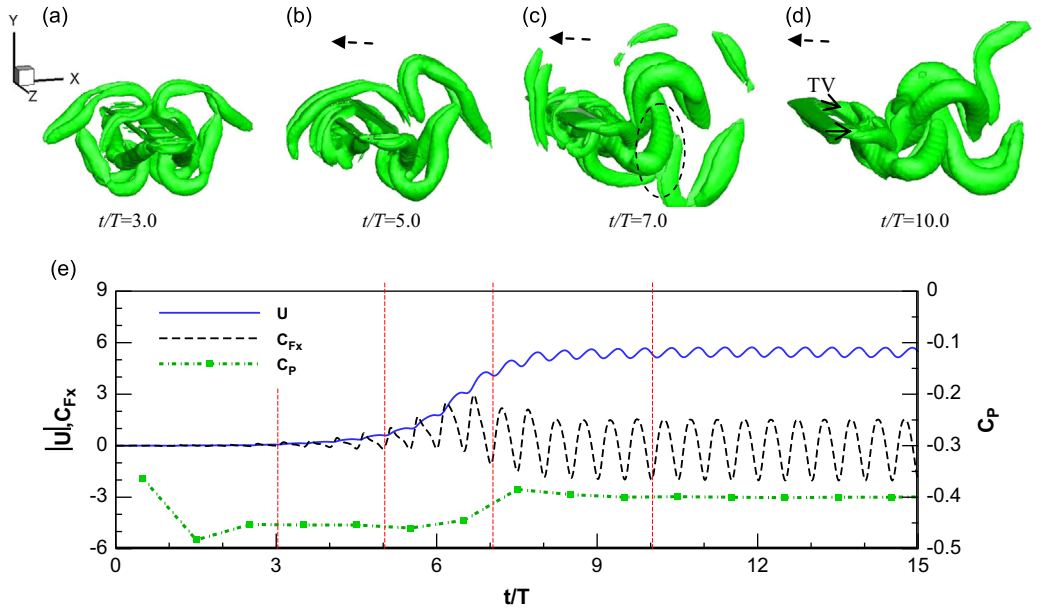

Fig. 8. Evolution process for a symmetric wing with AR=4.0, Re_{fr}=80, σ=4.0. (a)–(d) Vortex topology (reflection in the *YZ* plane) at four instants (solid arrows present velocities of tip vortex (TV)); (e) instantaneous horizental velocity, fluid force and the cycle-averaged-input power coefficient.

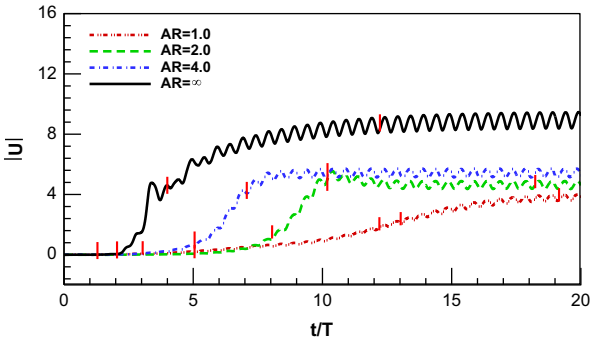

Fig. 9. Time variation of instantaneous horizontal velocity for wings with AR=1.0, 2.0, 4.0 and ∞, Re_{fr}=80, σ=4.0 (red solid lines present instants at different evolution stages). (For interpretation of the references to color in this figure caption, the reader is referred to the web version of this paper.)

magnitude of cycle-averaged-input power increases dramatically when the flow loses symmetry, but then returns to a constant at the stable state. The negative values indicate an input power on foil and wing.

The evolution process develops similarly but the quantities of final velocity, forces vary under different aspect ratios. Therefore, it is necessary to carry out a parametric study on understanding the 3-D mechanisms.

3.2. Aspect ratio effect

In this section, we further present the effect of aspect ratio on translational locomotion ability. Horizontal velocity variation of wings with different aspect ratios (AR) is plotted in Fig. 9, where evolution has reached an unsteady but stable state. It indicates that wings with bigger aspect ratios can induce faster velocities. The investigation by variation of horizontal fluid force coefficient (Fig.10) tells that there exists significant increase in the amplitude of thrust coefficient for wings with bigger aspect ratios. A similar phenomenon observed on U and C_{Fx} curves is that they both oscillate at the same frequency as the prescribed plunging motion. Referring to Eq. (2), translational velocity u_b is a function of translational force. Therefore stronger forces can lead to faster velocities, which is consistent with the trend of velocity and force curves in Figs. 9 and 10.

Instant wake topology of wings with AR=2.0 and 1.0 is presented in Figs. 11 and 12, along with Figs. 7 and 8, showing a flow structure variation under different aspect ratios. During evolution, there occurs similar phenomena, such as all the wake patterns go through the symmetry breaking down process, form vortex dipoles (as dashed circle lines), and achieve quasi-steady locomotion status. As they are all under the same flapping motion (Re_{fr}=80 and h=0.5), the rings in each set

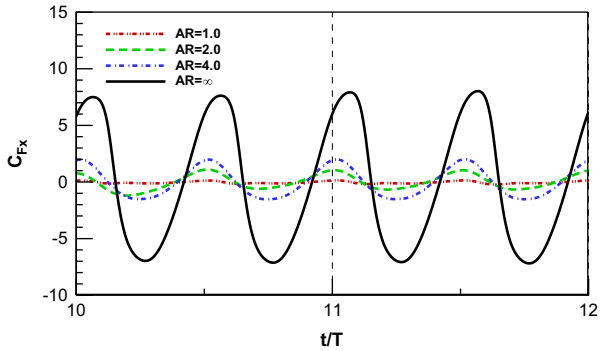

Fig. 10. Time variation of instantaneous horizontal fluid force coefficient for wings with AR=1.0, 2.0, 4.0 and ∞, Re_{fr}=80, σ=4.0 (C_{Fx} curves with AR=1.0 and 4.0 are the reflection in the *X*-axis.).

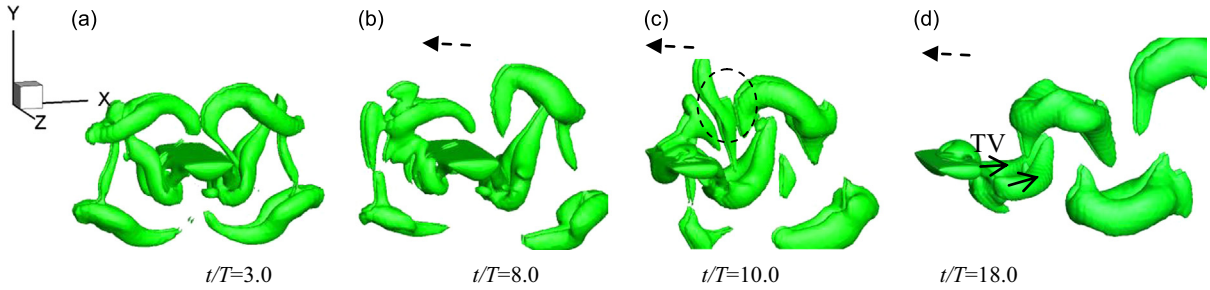

Fig. 11. Vortex topology at four instants for the wing with AR=2.0, Re_{fr}=80, σ=4.0.

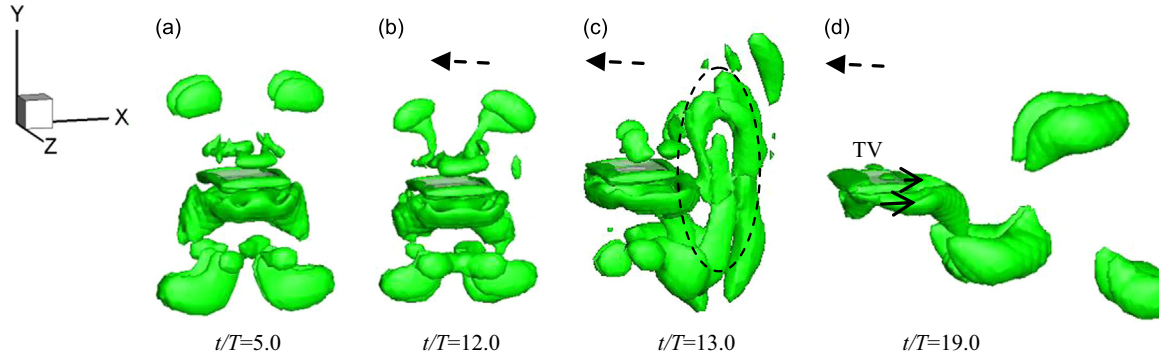

Fig. 12. Vortex topology (reflection in the *yz* plane) at four instants for the wing with AR=1.0, Re_{fr}=80, σ=4.0.

have the same direction of rotation and the oblique angles are similar. However, they exhibit qualitative differences under different AR. The 3-D rings are formed by tip-vortices (TV, as solid arrow marked in the figures) released from the span-wise tips. Wings with short aspect ratios AR=1.0 and 2.0 produce circular vortex rings, as the TV are close to each other along a short aspect distance. For wing with AR=4.0, the tip-vortices are not well merged resulting in the vortex shape being stretched thinner, forming elongated loops. Generally, the latter structure is beneficial to generating stronger jet flow, reducing energy dissipation, and thus facilitating a faster traveling speed.

The relation of the averaged translational Reynolds number (Re_u) responding to frequency Reynolds number (Re_{fr}) and aspect ratio (AR) is presented in Fig. 13(a). Firstly, for all cases, the Re_u increases monotonically with Re_{fr}. Such a behavior is well documented in the previous studies for 2-D self-propelled flapping foils (Alben and Shelley, 2005; Dong et al., 2006; Lu and Liao, 2006; Benkherouf et al., 2011). Secondly, Re_u turns into a linear function of Re_{fr} when Re_{fr} is over a critical value, ranging from 40 to 60 in the current study, which agrees with the study of Vandenberghe et al., (2004). Furthermore, induced velocity becomes larger as the aspect ratio increases at fixed Re_{fr}. Wing with small aspect ratio (AR=0.5) wanders very slowly, but the speed rises dramatically when aspect ratio is bigger than 1.0. It is noticeable that the translational speeds increase fast in the ranges of AR=2.0–4.0, and AR=6.0–∞.

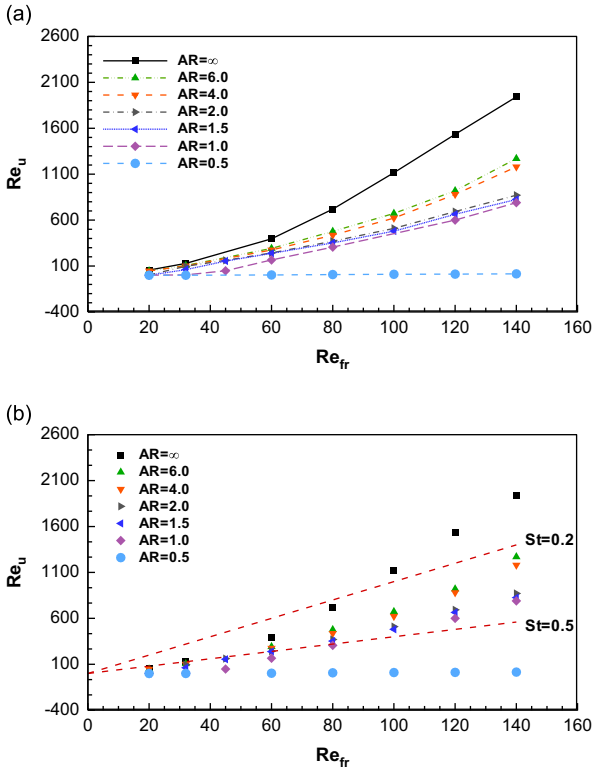

Fig. 13. Averaged translational Reynolds number (Re_u) against frequency Reynolds number (Re_{fr}) under various aspect ratios AR, with (a) trend lines and (b) Strouhal number range.

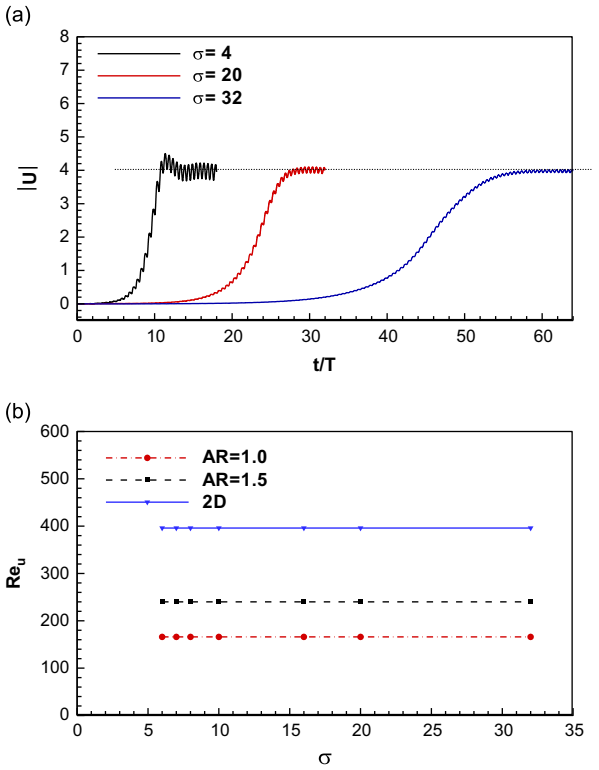

Fig. 14. (a) Variation of the instantaneous translational velocity U, AR = 1.5; (b) translational Reynolds number Re_u with different density ratios σ (Re_{fr} = 60).

The relationship of Re_{fr}, Re_u and St is shown in Fig. 13(b) for a fixed $\sigma=4.0$. The present simulations indicate that low-aspect-ratio wings lead to the same St as large-aspect-ratio ones under stronger flapping frequencies. Besides, the Strouhal number (St) mostly appears within the interval 0.2–0.5. This is an interval within which flying and swimming animals, driven by wing or tail, are likely to achieve and maintain high propulsive efficiency. Faster speeds can be achieved, considering the hydrodynamic performances alone, by wings with larger aspects-ratio. However, if applied to animals, penalties can be incurred by the wings for large aspect ratios, for example, the need to hold bending moments from stronger and heavier body structures. Therefore, an optimal range is selected in AR=2.0–4.0, within which the wings travel faster under a potentially high propulsive efficiency, coinciding with the study by Dong et al. (2006) which showed that most fish pectoral fins are found to have an aspect-ratio somewhere between 2.0 and 3.0.

3.3. Density ratio effect

According to the previous study on 2-D foils, self-propelled foil evolution motion and velocity magnitude are dependent on mass ratio σ. There is a critical density ratio, over which foil achieves a steady net movement in one direction rather than undergoes a spontaneous forward and backward motion (Alben and Shelley, 2005; Lu and Liao, 2006). In the present study, the focus is on the induced translational velocity eventually in steady status, thus relatively large mass ratios are selected as 4, 20 and 32.

The evolution of the instantaneous Re_u is shown in Fig. 14(a) with $Re_{fr}=60$. As seen, wings reach a similar final average velocity after initial evolution cycles. The ones with large mass ratio take more cycles to achieve the quasi-steady velocity, and have smaller fluctuations. This shows that the heavy wings are not as sensitive to the surrounding instantaneous fluid as light wings. In the stability aspect, the heavy ones are more stable. However they are less flexible in terms of their maneuverability.

More tests were carried out on wings with various density ratio and aspect ratios. Results in Fig. 14(b) show that the horizontal speed stays constant within little disturbance, and similar observation hold for those wings with either big or small aspect ratios. The dynamics of aquatic animals involves a complicated interaction of their bodies with the surrounding fluid flow. Usually, real tail or wing of swimming and flying animals has a density ratio range of $\sigma=10$–1000, and the flapping mode can naturally stay in the regime of a steady movement state to generate a forward flapping flight.

3.4. Perturbation effect

As described in Section 3.1, the symmetric foil and wing can travel horizontally with unidirectional locomotion, in either left or right with equal probability. During the evolution process, the initial perturbation plays an essential role on determining the way in the transition period. It is interesting to examine how the self-propelled phenomenon is influenced by initial flow and geometric conditions. In the present study, the effects of mesh symmetry and imposed perturbation velocities are examined respectively.

The induced moving directions of selected wings under different AR and Re_{fr} are summarized in Table 2. It clearly indicates that the wings with same aspect ratios are likely to be moving in the same direction, regardless of Re_{fr}. Even though the grid asymmetry is carefully avoided when we generate meshes, there are still slight differences between wings – left and right – over the whole computational domain and it may lead to a small perturbation and stimulate symmetric breakdown. The results shown in Table 2 could be attributed to the fact that the mesh is the same with an identical aspect ratio that results in the same direction.

Three cases with AR=∞, 1.5 and 1.0 are selected by simply swapping the left and right mesh domain, and the time evolutions of wing velocity are shown in Fig. 15. Obviously, the translational velocities are the same apart from the opposite moving directions, showing that the moving direction is sensitive to the initial mesh conditions.

Motivated by the methodology on the symmetry breaking of circular cylinder′s wake vortices (Tang and Aubry, 1997), and dynamic stability analysis of flying animal (Gao et al., 2011), the induced motion is studied by the imposition of an initial perturbation. In order to do this, small specified perturbation velocities (u_p) are imposed on the selected wings as an initial condition of velocity. The u_p is specified with an opposite direction as those without perturbation velocity cases (baseline cases), and various velocity magnitudes, with $u_p=0.00167\%$, 0.167% and 16.7% of the vertical angular velocity ($u_v=hc\omega/2\pi$). The results of the instantaneous velocity evolution process are shown in Fig. 15. It can be seen that the effect of u_p on wings with different AR shows a non-linear stability. There exists smaller u_p ($u_p/u_v=0.167\%$) which is not strong enough to alter

Table 2
Directions of induced velocities. $<+>$ represents wing travels in positive x direction, and $<->$ represents wing travels in negative x direction.

Re_{fr}\AR	∞	0.5	1	1.5	2	4	6
80	−	−	+	+	−	+	+
60	−	−	+	+	−	+	+
45			+	−	−		
32	−	−	+	−	−	+	+
20	−	+	+	−	−	+	+

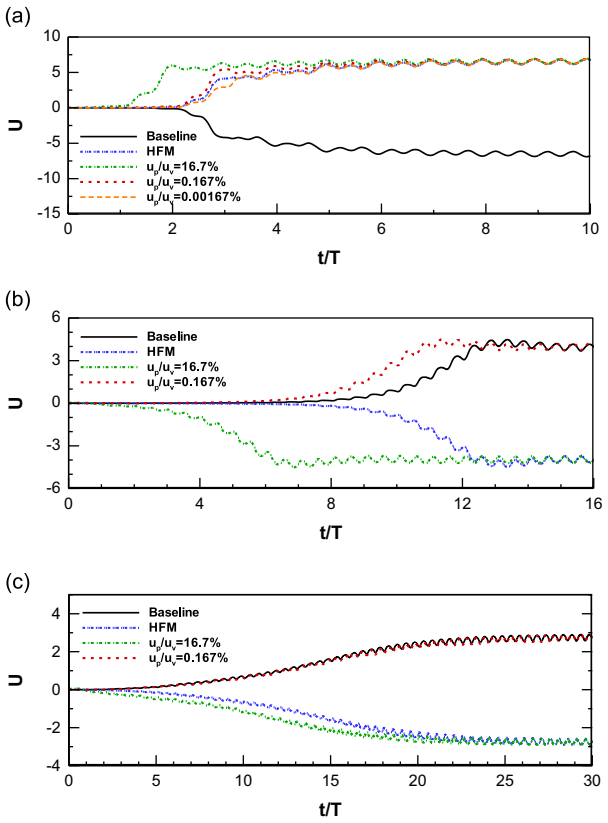

Fig. 15. Initial pertubation effect on movement directions of flapping wings, by testing horizontally flipped mesh (HFM) and various perturbation velocities (up) with (a) AR= ∞; (b) AR= 1.5; (c) AR=1.0. (Re_{fr}=60).

the horizontally moving direction as for cases with AR=1.0 and 1.5, and the bigger one (u_p/u_v=16.7%) which is able to change the traveling direction for all these three cases. The imposed perturbation affects the wing moving direction as well as the initial development time to reach the final quasi-steady status.

Generally, it can be seen that the perturbation has no effect on final quasi-steady velocity amplitude, but clearly has some effect on traveling direction and evolution process. To explain this phenomenon, it is deemed that the perturbation effects are mainly valid at the beginning of the transition period. Since the initial fluid flow is quiescent, and there is no horizontal constraint, the symmetric foil/wing is highly sensitive to the surrounding environment. Thus, small perturbation is able to lead to locomotion (as the status in Figs. 7 and 8(b)). However, after vortex collision (status in Figs. 7 and 8(c)), relatively stronger hydrodynamic forces are produced, hence those very small perturbation can be negligible, and would not change the velocity in the final quasi-steady status. This perturbation phenomenon influence may also be explained by a passive mechanism flapping counter torque (FCT) (Hedrick et al., 2009; Faruque and Humbert, 2010a, 2010b), and flapping counter force (FCF) (Cheng et al., 2009). They suggested that symmetric flapping wings produced restoring torque and force making swimmers respond to perturbation by decreasing body rotation, and could maintain flight stability by a passive damping coefficient. Therefore, the periodic plunging motion in the current study is able to maintain a stable locomotion status after slightly initial perturbation.

4. Conclusions

The locomotion of a prescribed plunging wing with one degree of freedom in lateral direction in stationary fluid has been studied systematically by a 3-D fluid-motion coupling method. The results show that the wing can break a left-right symmetric status under the prescribed heaving motion, and achieve a quasi-steady locomotion horizontally. The 3-D effect with various aspect ratios (AR) on the induced flow phenomenon and translational velocities has been investigated. It indicates that the induced translational velocity increases with large AR, and the Strouhal number (St) reasonably ranges between 0.2 and 0.5. Under a comprehensive consideration, the optimal AR on such a self-propelled model with 1-DoF is suggested in the range of 2.0–4.0. Moreover, it is clear that the density ratio (σ) plays a role in rapid transition during evolution procedure. The lighter wings are more sensitive to the surrounding fluid environments. Furthermore, it is shown that the translational traveling direction can be controlled by imposing an initial perturbation velocity with certain magnitude.

References

Alben, S., Shelley, M., 2005. Coherent locomotion as an attracting state for a free flapping body. Proceedings of the National Academy of Sciences 102 (32), 11163–11166.

Benkherouf, T., Meckadem, M., Oualli, H., Hanchi, V., Keirsbulck, L., Labraga, L., 2011. Efficiency of an auto-propelled flapping airfoil. Journal of Fluids and Structures 27 (4), 552–566.

Cheng, B., Fry, S.N., Huang, Q., Deng, X., 2009. Aerodynamics damping during rapid flight maneuvers in the fruit fly Dorsophila. Journal of Experimental Biology 213, 602–612.

Combes, S.A., Daneil, T.L., 2001. Shape, flapping and flexion: wing and fin design for forward flight. Journal of Experimental Biology 204, 2073–2085.

Drucker, E.G., Lauder, G.V., 1999. Locomotion forces on a swimming fish: three-dimensional vortex wake dynamics quantified using digital particle image velocimetry. Journal of Experimental Biology 202, 2393–2412.

Dong, H., Mittal, R., Najjar, F.M., 2006. Wake topology and hydrodynamic performance of low-aspect-ratio flapping foils. Journal of Fluid Mechanics 566, 309–343.

Faruque, I., Humbert, J.S., 2010a. Dipteran insect flight dynamics. Part 1: longitudinal motion about hover. Journal of Theoretical Biology 264, 538–552.

Faruque, I., Humbert, J.S., 2010b. Dipteran insect flight dynamics. Part 2: lateral-directional motion about hover. Journal of Theoretical Biology 265, 306–313.

Gao, N., Aono, H., Liu, H., 2011. Perturbation analysis of 6DoF flight dynamics and passive dynamic stability of hovering fruit fly Drosophila melanogaster. Journal of Theoretical Biology 270, 98–111.

Guerrero J., 2009. Numerical Simulation of the Unsteady Aerodynamics of Flapping Flight (Thesis for the degree of Doctor of Philosophy). Department of Civil, Environmental and Architectural Engineering, University of Genoa.

Heathcote, S., Gursul, I., 2007. Flexible flapping airfoil propulsion at low Reynolds numbers. AIAA Journal 45 (5), 1066–1079.

Hedrick, T.L., Cheng, B., Deng, X., 2009. Wingbeat time and the scaling of passive rotational damping in flapping flight. Science 324, 252–255.

Hu, J.X., Xiao, Q., Incecik, A., 2011. Dynamic response of a flapping foil with a non-sinusoidal kinematic motion. In: Proceedings of the 21st International Offshore and Polar Engineering Conference (ISOPE), p. 239.

Lewin, G.C., Hajhariri, H., 2003. Modelling thrust generation of a two-dimensional heaving airfoil in a viscous flow. Journal of Fluid Mechanics 492, 339–362.

Lu, X.Y., Liao, Q., 2006. Dynamic responses of a two-dimensional flapping foil motion. Physics of Fluids 18, 098104.

Miller, L.A., Peskin, C.S., 2004. When vortices stick: an aerodynamic transition in tiny insect flight. Journal of Experimental Biology 207, 3073–3088.

Spagnolie, S.E., Moret, L., Shelley, M.J., Zhang, J., 2010. Surprising behaviors in flapping locomotion with passive pitching. Physics of Fluids 22, 041903.

Tang, S., Aubry, N., 1997. On the symmetry breaking instability leading to vortex shedding. Physics of Fluids 9, 2550–2561.

Tian, F.-B., Luo, H., Song, J., Lu, X.-Y., 2013. Force production and asymmetric deformation of a flexible flapping wing in forward flight. Journal of Fluids and Structures 36, 149–161.

Triantafyllou, G.S., Triantafyllou, M.S., Grosenbaugh, M.A., 1992. Optimal thrust development in oscillating foils with applications to fish propulsion. Journal of Fluids and Structures 7, 204–224.

Vandenberghe, N., Zhang, J., Childress, S., 2004. Symmetry breaking leads to forward flapping flight. Journal of Fluid Mechanics 506, 147–155.

Vandenberghe, N., Childress, S., Zhang, J., 2006. On unidirectional flight of a free flapping wing. Physics of Fluids 18, 014102.

Visbal, M., Yilmaz, T.O, Rockwellm, D., 2013. Three-dimensional vortex formation on a heaving low-aspect-ratio wing: computations and experiments. Journal of Fluids and Structures 38, 58–76.

Walker, J.A., Westneat, M.W., 2002. Performance limits of libriform propulsion and correlates with fin shape and motion. Journal of Experimental Biology 205, 177–187.

Xiao, Q., Liu, W., Hu, J.X., 2011. Parametric study on a cylinder drag reduction using downstream undulating foil. European Journal of Mechanics — B/Fluids 36, 48–62.

Xiao Q., Hu J.X., Liu H., 2014. Role of flexibility and inertia on the dynamics of low-aspect-ratio flapping wings. Bioinspiration and Biomimetics 9, 016008 (15pp), http://dx.doi.org/10.1088/1748-3182/9/1/016008.

Young, J., Lai, C.S., 2007. Mechanisms Influencing the efficiency of oscillating airfoil propulsion. AIAA Journal 45 (7), 1695–1702.

Zhang, J., Liu, N.-S., Lu, X.-Y., 2010. Locomotion of a passive flapping flat plate. Journal of Fluid Mechanics 659, 43–68.